Anal. Bioanal. Electrochem., Vol. 10, No. 2, 2018, 269-280

Analytical & Bioanalytical Electrochemistry

Full Paper

One-pot Electrochemical Preparation and Characterization of High Surface Area Ultrafine CeO_2 Nanoparticles

Mustafa Aghazadeh and Ali Ahmadi*

Materials and Nuclear Research School, Nuclear Science and Technology Research Institute (NSTRI), P.O. Box 14395-836, Tehran, Iran

*Corresponding Author, Tel.: +98-21-82064289
E-Mail: amahmadi@aeoi.org.ir

Received: 30 November 2017 / Accepted: 18 February 2018 / Published online: 28 February 2018

Abstract- Cerium oxide possess various applications including waste refiner, catalyst, electrolyte in solid state fuel cell, glass decoloring and materials polishing. The use of this material in nanosized form, with high surface area improves its functionality significantly. In this study, ultrafine CeO_2 nano-particles were prepared by a simple electrochemical platform. The synthesis experiments were performed from 0.01 M cerium nitrate aqueous electrolyte in the presence of H_2O_2 and PVP. The as-deposited powder was also calcined 400 °C for 2 h. The morphologies and crystal structures of the prepared powders were examined by means of scanning and transmission electron microcopies (SEM and TEM) as well as X-ray diffraction (XRD), FT-IR and DSC-TGA. These analysis results proved the electro-synthesis of pure crystalline cerium oxide final particles. The high surface area (184.8 $m^2 g^{-1}$) of the prepared nanoparticles was also confirmed through BET analysis. A possible mechanism of CeO_2 deposition on the cathode surface was proposed, when the hydrogen peroxide additive played an important role in the formation of hydrous cerium oxide. In final, this simple electrochemical procedure is proposed for mass production of high surface area ultrafine nanoparticles of cerium oxide.

Keywords- Electrodeposition, Cerium Oxide, Heat-treatment, Nanoparticles

1. INTRODUCTION

Rare-earth oxide nanoparticles (NPs) have attracted attention due to their excellent catalytic properties and their possible applications in biological fields. Among these oxides, ceria (CeO_2) has attracted considerable interest as a promising material in technological

applications including polishing materials, catalysts, oxygen sensors, corrosion protection and UV-blocking filters [1]. This is because of its high refractive index, chemical stability, mechanical hardness, high dielectric constant, and high transparency in the visible and near-IR region. Furthermore, its high photo- and thermos-catalytic activities are attractive as an anode material for photo-electrolysis of water and fuel cells, respectively [2]. Recently, cerium oxide has found interested candidate in bio-logical and bio-medical applications [4,5]. To enhance the cerium oxide performance in the above applications, high surface area nanostructured CeO_2 has been proposed. Hence, preparation of the ultrafine mono-dispersed cerium oxide particles in large-scale is an interesting research area.

Up to now, physical and chemical techniques such as hydrolysis [5], microwave [6], solvothermal [7], hydrothermal [8], co-precipitation [9] and electrodeposition [10-13] methods have been employed for synthesis of different nano-structures of CeO_2. Electrodeposition is a facile alternative attractive route for the deposition of thin films and nano-powders of metal oxides/hydroxides due to its capability in controlling the physic-chemical properties of the deposited materials and also producing thick and crack-free films on various substrates [14-21]. Compared to other methods applied for the fabrication of nanostructured CeO_2, electrodeposition appears to be a simple, effective, and highly sensitive [22-25]. This method has received more and more attentions due to its inexpensive equipment, simple procedure and low processing temperature, controlled thickness of the film and low cost process.

In the cathodic electrolytic deposition, hydroxide ions are formed at an electrode surface by a cathodic process and metal ions or complexes are then hydrolyzed by the electrogenerated base. For example, Arurault et al. [22], Zhitomirsky et al. [23,24] and Creuset al. [25] have reported deposition of thin cerium oxide films from a solution of Ce(III) nitrate. It was also found that the base (OH^-) electrogeneration results the formation of colloidal particles of $Ce(OH)_3$ or CeO_2 nH_2O [13,22], or also the formation of $Ce(OH)_2^{2+}$ cations on the cathode surface, which can be hydrolyzed into cerium oxide. Furthermore, hydrogen peroxide (H_2O_2) as an additive has been used in the electro-synthesis of ceria thin films [22-24], where it prevents the accumulation of nitrite or ammonia ions that provokes deposition instabilities, and leads to more adherent and uniform oxide films [24,25]. Reviewing these works indicates that most of the electrochemical studies (i.e. both anodic and cathodic) have focused on the preparation of crack-free cerium oxide thin films or coatings. However, electrochemical preparation of cerium oxide nanopowder has been rarely reported. Notably, it was reported that very fine nano-particles of metal oxides and hydroxides can be prepared through cathodic electro-synthesis [26-30]. Here, we introduce a facile electrochemical route for mass production of ultrafine cerium oxide nanoparticles in powder form. In fact, high surface area ultra-fine cerium oxide nanoparticles (NPs) are fabricated from cerium nitrate aqueous solution using cathodic electrosynthesis procedure.

The prepared NPs are also characterized through various techniques of XRD, IR, SEM, TEM, DSC-TGA and BET.

2. MATERIALS AND METHODS

2.1. Chemicals

Commercial purity cerium nitrate hexahydrate [$Ce(NO_3)_3.6H_2O$ (Merck), 99.9%], hydrogen peroxide (H_2O_2, 30 wt.% in water, Sigma Aldrich) and polyvinylpyrrolidone (PVP, $(C_6H_9NO)_n$, Mw=360,000) was used as starting material in the electro-synthesis experiments. All materials were used as received and without any purification.

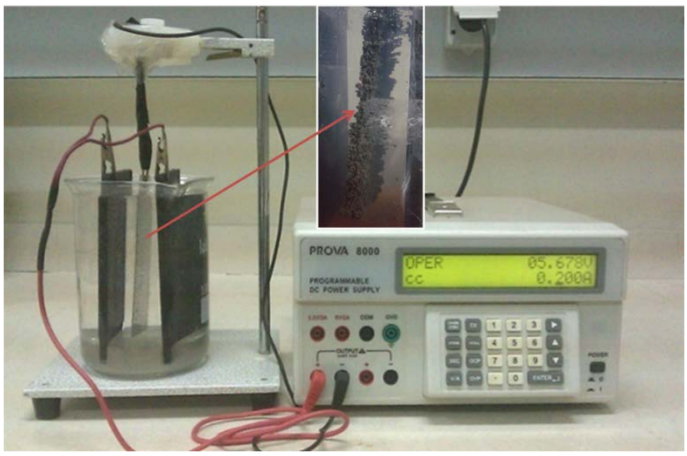

Fig. 1. Electrochemical set up used for the preparation of cerium oxide. The inset shows the formed black deposit on the cathode surface at the end of deposition run

2.1. Sample preparation

The electrochemical experiments proceeded in a simple two-electrode electrochemical cell previously used for electro-synthesis of iron oxide nanoparticles [31-33]. The electrochemical cell includes a stainless steel cathode (316 L, 100×50×0.5 mm) centered between two parallel graphite counter electrodes, as shown in Fig. 1. The deposition bath contains 1litter mixed solution of 0.2 M $Ce(NO_3)_3.6H_2O$, 0.025 M H_2O_2 and 1 g/L PVP. All electro-synthesis runs were carried out in the constant current (i.e. galvanostatic) with applying current density of 20 mA cm^{-2} at room temperature. After deposition step, the steel cathode was removed from the deposition bath, and washed several times with deionized water. The deposited film was then scraped from the steel cathode, and the resulted wet powder was washed and dispersed in ethanol and centrifuged at 6000 rpm for 20 min in order to removal of adsorbed PVP into the deposit powder surface. In final, the powder was dried at 60 ^oC for 1h and the obtained dry powder was collected and named electrodeposited sample.

Also, this sample was calcined at 400 ^{o}C for 2 h and the calcined powder was named final oxide product. It should be noted that the used steel electrode had surfaces area as high as 100 cm^2, and we were able to obtain about 4-5 g of deposit after each deposition. Hence, this simple electrochemical system can be easily scaled up only using large steel and graphite plates to mass production of cerium oxide.

2.1. Characterizations

The phase and crystal structure of the samples were determined by X-ray diffraction (XRD) with a diffractometer (Phillips PW-1800) using monochromatized Cu Kα radiation at a scanning speed of 0.5^{o} min^{-1}. Thermogravimetric analysis (TGA) and thermal behaviors of as-deposited samples were investigated by means of differential scanning calorimeter (DSC, STA-1500). The morphology of the samples was examined using a scanning electron microscopy (Philips 515). Transmission electron microscopy (TEM) images were taken using a Zeiss EM900 with an accelerating voltage of 80 kV. FT-IR spectrum was provided through a Bruker Vector 22 FT-IR spectrometer within the wave numbers of 400-4000 cm^{-1}. The measurement of surface area of the prepared nanopowder was obtained through measuring N_2 adsorption–desorption isotherms at 77 K with a Quanta-chrome NOVA-2200e system.

3. RESULTS AND DISCUSSION

3.1. Mechanism of cerium oxide formation

Electrochemical mechanism of base electrogeneration during cathodic deposition has been widely discussed in the literature [13,22-24,34]. In the case of nitrate bath, where anions could participate in cathodic reaction, the hydroxyl ions are then produced by the reduction of nitrate ions (Eqs. (1-2)) [22,35], as listed below:

$$NO_3^- + 7H_2O + 8e^- \rightarrow NH_4^+ + 10OH^- \quad (1)$$

$$NO_3^- + H_2O + 2e^- \rightarrow NO_2^- + 2OH^- \quad (2)$$

Furthermore, the dissolved oxygen and water molecules can be reduced to generate base ions on the cathode surface (Eqs. 3-4) [35]:

$$O_2 + H_2O + 4e^- \rightarrow 4OH^- \quad (3)$$

$$2H_2O + 2e^- \rightarrow H_2 + 4OH^- \quad (4)$$

On the other hand, the addition of hydrogen peroxide leads to the formation of supplementary hydroxyl ions during the cathodic reaction (Eq. (5)) [24,25]:

$$H_2O_2 + 2e^- \rightarrow 2OH^- \quad (5)$$

With increasing the pH on the cathode surface as a result of the above mentioned reactions, cerium ions move toward cathode surface and are chemically reacted with base ions to form cerium hydroxide (Eq. (6)):

$$Ce^{3+} + 3OH^- \rightarrow Ce(OH)_3 \downarrow \quad (6)$$

It was showed that the role of H_2O_2 as a precursor was to prevent the formation of a nonstoichiometric cerium oxide deposit through oxidizing Ce^{3+} into Ce^{4+}, the latter being more easily hydrolyzed [24,25]:

$$Ce^{3+} + 2OH^- \rightarrow Ce(OH)_2^{2+} + e^- \quad (7)$$

Furthermore, it has been found that hydrogen peroxide precursor improves the adherence and uniformity of the oxide films [25]. The formation of hydroxyl ions at the cathode leads to a local increase of the pH at the surface that promotes the formation of a $Ce(OH)_3$ precipitate or/and the formation of a soluble ionic complex $Ce(OH)_2^{2+}$. Notably, the $Ce(OH)_2^{2+}$cations can be also preferentially formed when H_2O_2 is present in the deposition bath.

$$2Ce^{3+} + 2OH^- + H_2O_2 \rightarrow 2Ce(OH)_2^{2+} \quad (8)$$

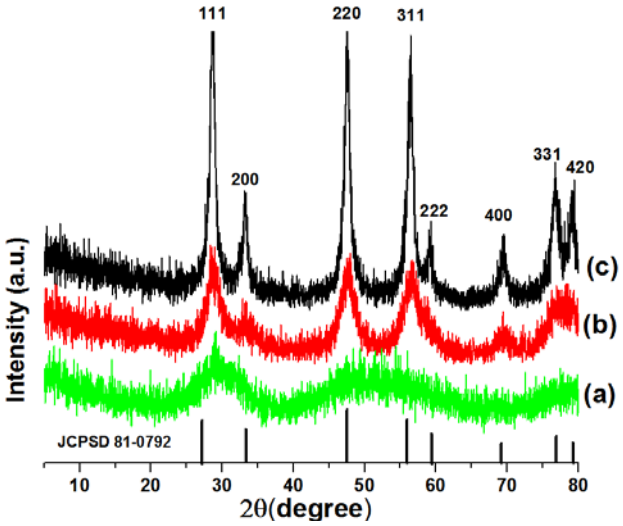

Fig. 2. XRD patterns of (a) as-electrodeposited and calcined samples at (b) 200 ^oC and (c) 400 ^oC

Finally, the cerium oxide deposits resulted either from the oxidation of $Ce(OH)_3$ (Eq. (6)) or from the hydrolysis of $Ce(OH)_2^{2+}$ (Eq. (8)) [24,25]:

$$Ce(OH)_3 \rightarrow CeO_2 + H_3O^+ + e^- \quad (9)$$

$$Ce(OH)_2^{2+} + 2OH^- \rightarrow CeO_2 + H_2O \quad (10)$$

Notably, the electrochemical mechanism of formation of these oxide films is really complex. However, considering the bath type and additive used in this work, the formation of cerium oxide through Eqs. (8 and 10) is more possible.

3.2. XRD

Fig. 2 shows the XRD patterns of the as-electrodepsoited and calcined cerium oxide samples. The XRD pattaern of the as-deposited sample in Fig. 1a has two main diffraction broad peaks. The former peak at about 2theta of 30^o is related to the (111) and (200) peaks of cerium oxide. The second broad peak exhibits two maxims at 2theta of 46^o and 57^o, which are corresponded to the (220) and (311) diffraction peaks of cerium oxide. The brosd peak and relative amorph form of the as-electrodeposited powder my due to the presenc of the water in the sample.Hence, this pattern can be indexted as CeO_2 nH_2O, and in agreement with the TG results (Fig. 3) and supprot the proposed mechanism. The calcined powder at 200 ^{o}C gives XRD peaks at (111), (200), (220), (311), (400) and (311), as clearly observable in Fig. 2b. This pattern has good agreement with diffraction lines of cubic cerium oxide with the JCPDS file No. 75-0076. For the calcined powder at 400 ^{o}C, eight peaks that are clearly distinguishable, which are (111), (200), (220), (311), (400), (331) and (422) peaks. All of these diffraction peaks could be indexed to a pure cubic fluorite structure of CeO_2 (space group: Fm3m) with lattice constant a=5.411Å, which is in agreement with the JCPDS file No. 75-0076. It is seen that as the calcination temperature is increased three more peaks at (222), (400) and (331) are formed, which implies the increment in crystallization in a face centered cubic structure. From these findings, the calcined powder at 400 ^{o}C was introduced as final cerium oxide sample.

Furthermore, verage particle size of the prepared cerium oxide powderswere estimated by Scherrer's equation [32]:

$$D_{hkl} = 0.9\lambda/\beta cos\theta \quad (11)$$

Where D_{hkl} is average particle size, λ the wavelength of CuKα radiation (0.15406 nm) and β the full width at half maximum (FWHM) and θ is Bragg's angle of the peak. Using this relation, the calculations give average crystallite sizes of 3.2 nm, 4.5 nm and 7.2 nm for the as-electrodeposited, calcined at 200 ^{o}C and 400 ^{o}C, respectively.

3.3. Thermal analysis

To better characterize the as-electrodeposited powder and determination of the physico-chemical changes during calcination at 400 ^{o}C, the DSC-TG analysis of the electrodeposited

powder was performed in the temperature range of 25 and 600 ^{o}C. Results of thermal analysis (DSC and related TG) of as-electrodeposited powder are presented in Fig. 3. In the DSC profile, only one endothermic peak at temperatures below 125^{o}C is observed. This peak is due to dehydration of free and physically absorbed molecular water/or ethanol associated with electrodeposited powder [25,34]. TG profile indicates 6.6% weight loss for this step, as seen in Fig. 3. After this step, there is no essential weight loss on the TG profile and no endo-/exo-thermic peak on the DSC profile of the as-electrodeposited powder. These observations implicated the oxide nature of the electrodeposited powder, and also presence of the water molecules on the surface of this powder. Hence, the chemical formula of CeO_2 .nH_2O can be proposed for the electrodeposited powder. This results in agreement with the XRD and IR findings and further support the proposed mechanism.

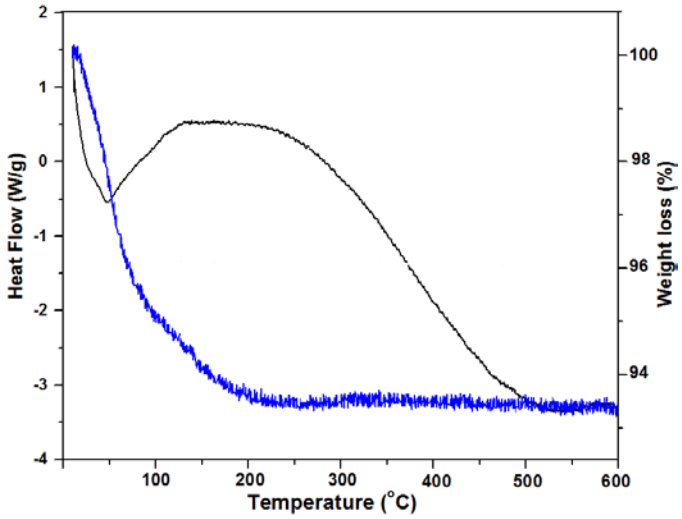

Fig. 3. DSC-TG analysis of the electrodeposited sample

3.4. IR

Fig. 4 presents the FTIR spectra of the as-electrodeposited and calcined powders. These spectra have several significant absorption peaks recorded in the range from 4000 to 400 cm^{-1}. The FTIR spectra show all principal vibrational modes, which are in good agreement with literature [35,36]. The absorption broad peak at 3500-4500 cm^{-1} is assigned to OH stretching vibrations of H_2O in the sample [37]. The absorption bands at 1047, 1475, 1380 and 1630 cm^{-1} correspond to different vibration modes of physically adsorbed water molecules, and the intercalated nitrate ion in the deposited powder [27,38]. The IR absorption bands at about 840 cm^{-1} and 512-7 cm^{-1} are related to the Ce-O stretching vibrations in both samples [35,36], and confirmed the cerium oxide of both powders.

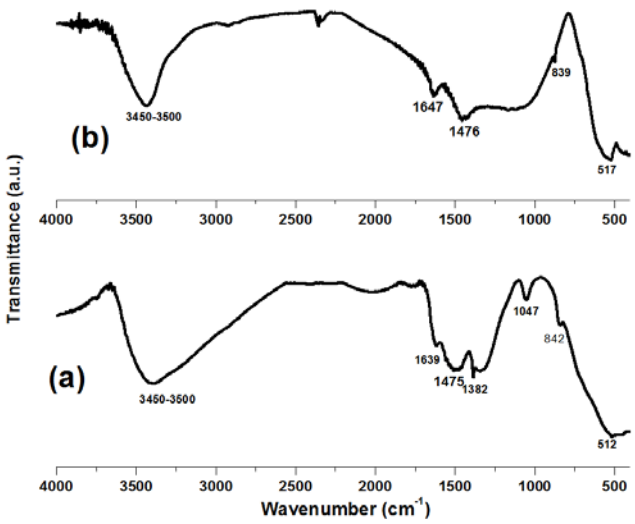

Fig. 4. IR spectra of (a) the as-electroposited and (b) final oxide powders

3.5. Morphological characterization

Fig. 5 shows the SEM images of the prepared powders before and after calcination. As clearly observable in Fig. 5, both powders have uniform spherical particle morphology at nano-scale. The sizes of the observed particles are very fine, where it could not be measured through these SEM images. For better observation, the high magnification TEM images were provided and presented in Fig. 6. TEM observations revealed that the as-electrodeposited powder exhibits well-dispersion and not-agglomerated form of the oxide powder. The size of electrodeposited particles was determined to be about 5nm (Fig. 6a).

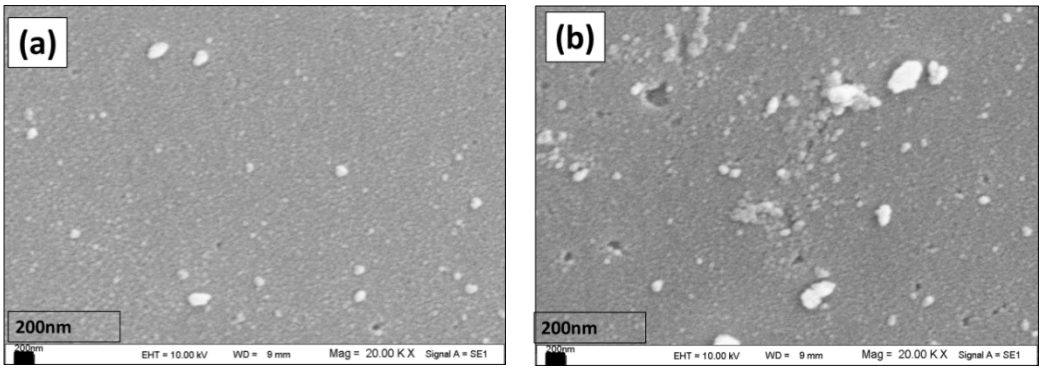

Fig. 5. SEM images of (a) the electrodeposited and (b) the calcined samples

For the calcined powder, spherical particles with size of ~5nm are also observed in the TEM image (Fig. 6b). These observations confirmed the preparation of ultrafine nanoparticles of cerium oxide through our applied simple electrochemical platform.

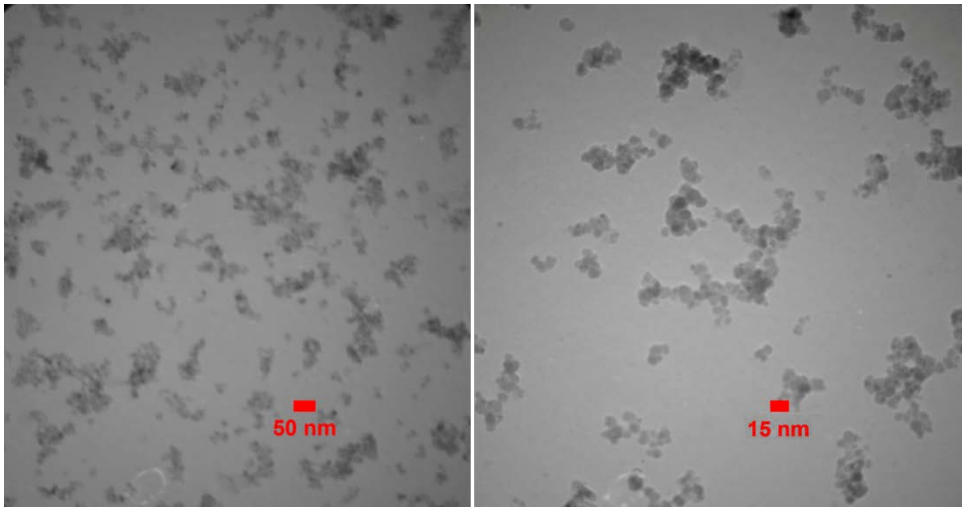

Fig. 6. TEM images of the prepared final cerium oxide

3.6. Surface area

Surface area is one of key factors determining in most applications of cerium oxide nanoparticles [2,3]. Hence, N_2 adsorption/desorption was used for the evaluation of the surface area of the prepared cerium oxide nanoparticles.

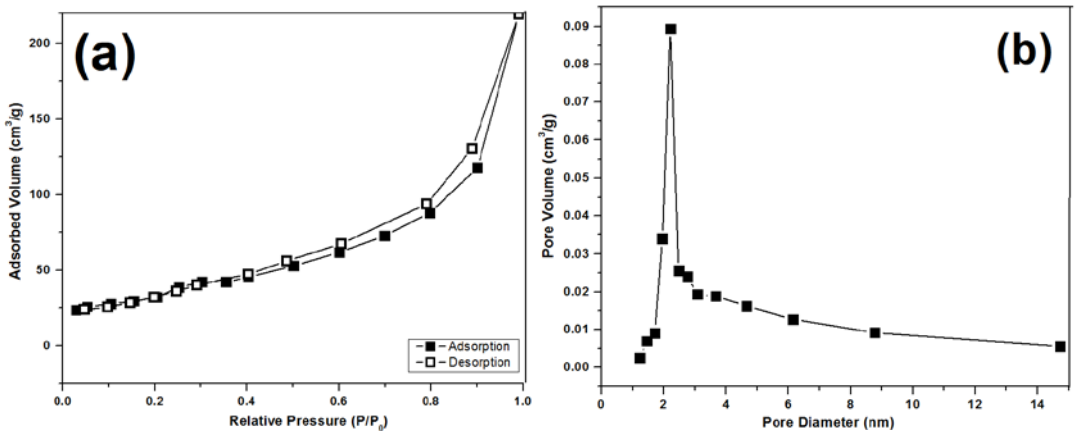

Fig. 7. (a) BET and (b) BJH pore size distribution curves of cerium oxide nanoparticle

Fig. 7 presents the nitrogen adsorption/desorption isotherm and the corresponding pore size distribution profile of the cerium oxide nanoparticles. The N_2 isotherm of CeO_2 nanoparticles has a typical type II form with a type H3 hysteretic loop, indicating the presence of micro-porous materials according to the IUPAC classification. The H3 type loops are generally given by the adsorbents with narrow size distribution of uniform pores. The plot of the pore-size distribution (Fig. 7b) was determined from the desorption branch of the isotherm using the Barrett–Joyner–Halenda (BJH) method. The mean pore diameter and the

Brunauer–Emmet–Teller (BET) surface area of the Fe_3O_4 nanoparticles were estimated to be 1.97 nm and 184.8 m^2 g^{-1}, respectively. According to the IUPAC classification, there are three classes of pore sizes: a) micropores of <2 nm; b) mesopores of 2-5 nm; and c) macropores of >5 nm. So, our prepared sample has micro-porous nature [39-41]. Notably the prepared cerium oxide nanoparticles exhibits high surface area of the 184.8 m^2 g^{-1}, which is very larger than the reported surface area for cerium oxide particles in the literature [13,22-25]. This improvement in the surface area of the cerium oxide nanoparticles is resulted from the important role of PVP in the deposition process [42,43], where lead to preparation of well-dispersed and uniform non-agglomerated nanoparticles (as seen in TEM images, Fig. 5). In fact, the PVP polymer on the cathode surface could prevent CeO_2 nanoparticles to agglomerated and enhance the surface area of the deposited product.

4. CONCLUSION

A simple and facile electrochemical route was developed for the production of cerium oxide nanopowder. Morphological and structural analyses through XRD, SEM and TEM confirmed the synthesis of spherical fine pure CeO_2 nanoparticles with size of 5 nm. DSC-TG analysis revealed only physical absorbed water on the chemical structure of the as-electrodeposited powder and confirmed its oxide nature. Based on the findings, the applied electrochemical platform in this work is introduced as facile method for fabrication of high surface area cerium oxide nanoparticles.

REFERENCES

[1] C. Walkey, S. Das, S. Seal, J. Erlichman, and K. Heckman, Environ. Sci. Nano 2 (2015) 33.

[2] T. Montini, M. Melchionna, M. Monai, and P. Fornasiero, Chem. Rev. 116 (2016) 5987.

[3] L. He, Y. Su, J. Lanhong, and S. Shi, J. Rare Earths 33 (2015) 791.

[4] F. Charbgoo, M. B. Ahmad, and M. Darroudi, Int. J. Nanomed. 20 (2017) 1401.

[5] S. J. Jeyakumar, T. Dhanushkodi, I. K. Punithavathy, and M. Jothibas, J. Mater. Sci. Mater. Electron. 28 (2017) 3740.

[6] B. S. Shirke, A. A. Patil, P. P. Hankare, and K. M. Garadkar, J. Mater. Sci. Mater. Electron. 22 (2011) 200.

[7] J. Liu, L. Yan, X. Chen, S. Wang, and C. Tian, J. Rare Earths 33 (2015) 892.

[8] H. Li, F. Meng, J. Gong, Z. Fan, and R. Qin, J. Mater. Sci. Mater. Electron. 28 (2017) 9584.

[9] M. Yue, M. Cui, N. Zhang, Z. Long, and X. Huang, J. Rare Earths 31 (2013) 251.

[10] R. J. La, Z. A. Hua, H. L. Li, X. L. Shang, and Y. Y. Yang, Mater. Sci. Eng. A 368 (2004) 145.
[11] T. Yousefi, A. N. Golikand, and M. H. Mashhadizadeh, Mater. Sci. Semicond. Process. 16 (2013) 1943.
[12] V. Lair, A. Ringuede, P. Vermaut, and S. Griveau, Phys. Stat. Sol. 5 (2008) 3492.
[13] P. Bocchetta, M. Santamaria, and F. D. Quarto, J. Appl. Electrochem. 39 (2009) 2073.
[14] M. Aghazadeh, and M. R. Ganjali, Ceram. Int. 44 (2018) 520.
[15] M. Aghazadeh, and M. R. Ganjali, J. Mater. Sci. 53 (2018) 295.
[16] M. Aghazadeh, Mater. Lett. 211 (2018) 225.
[17] M. Aghazadeh, M. R. Ganjali, and P. Noruzi, Thin Solid Films 634 (2017) 24.
[18] M. Aghazadeh, I. Karimzadeh, and M. R. Ganjali, Phys. Status Solidi A 214 (2017) 1700365.
[19] M. Aghazadeh, I. Karimzadeh, and M. R. Ganjali, J. Mater. Sci. 28 (2017) 19061.
[20] M. Aghazadeh, and I. Karimzadeh, Mater. Res. Express 4 (2017) 105505.
[21] M. Aghazadeh, and A. Ahmadi, Anal. Bioanal. Electrochem. 9 (2017) 469.
[22] L. Arurault, P. Monsang, J. Salley, and R. S. Bes, Thin Solid Films 466 (2004) 75.
[23] I. Zhitomirsky, and A. Petric, Mater. Lett. 40 (1999) 263.
[24] I. Zhitomirsky, and A. Petric, Ceram. Int. 27 (2001) 149.
[25] J. Creus, F. Brezault, C. Rebere, and M. Gadouleau, Surf. Coatings Technol. 200 (2006) 4636.
[26] M. Aghazadeh, I. Karimzadeh, M. R. Ganjali, and A. Behzad, J. Mater. Sci. Mater. Electron. 28 (2017) 18121.
[27] M. Aghazadeh, A. A. M. Barmi, and M. Hosseinifard, Mater. Lett. 73 (2012) 28.
[28] M. Aghazadeh, A. N. Golikand, and M. Ghaemi, Int. J. Hydrogen Energy 36 (2011) 8674.
[29] M. Aghazadeh, A. A. M Barmi, D. Gharailou, M. H. Peyrovi, and B. Sabour, Appl. Surf. Sci. 283 (2013) 871.
[30] A. Barani, M. Aghazadeh, M. R Ganjali, B. Sabour, A. A. M. Barmi, and S. Dalvand, Mater. Sci. Semicond. Process. 23 (2014) 85.
[31] M. Aghazadeh, I. Karimzadeh, M. R. Ganjali, and M. MohebiMorad, Mater. Lett. 196 (2017) 392.
[32] M. Aghazadeh, I. Karimzadeh, T. Doroudi, M. R. Ganjali, and P. H. Kolivand, Appl. Phys. A 123 (2017) 529.
[33] M. Aghazadeh, I. Karimzadeh, and M. R. Ganjali, J. Mater. Sci. Mater. Electron. 28 (2017) 13532.
[34] M. Aghazadeh, and M. Hosseinifard, Ceram. Int. 39 (2013) 4427.
[35] S. Thakur, and P. Patil, Sens. Actuator B 194 (2014) 260.

[36] A. Umar, R. Kumar, M. S. Akhtar, G. Kumar, and S. H. Kim, Colloid Interface Sci. 454 (2015) 61.
[37] M. Aghazadeh, M. Hosseinifard, B. Sabour, and S. Dalvand, Appl. Surf. Sci. 287 (2013) 187.
[38] J. Tizfahm, M. Aghazadeh, M. Ghannadi Maragheh, M. R. Ganjali, P. Norouzi, and F. Faridbod, Mater. Lett. 167 (2016) 153.
[39] M. Aghazadeh, M. Asadi, M. G. Maragheh, M. R. Ganjali, P. Norouzi, and F. faridbod, Appl. Surf. Sci. 364 (2016) 726.
[40] M. Aghazadeh, J. Appl. Electrochem. 42 (2012) 89.
[41] M. Aghazadeh, M. Ghaemi, B. Sabour, and S. Dalvand, J. Solid State Electrochem. 18 (2014) 1569.
[42] K. M. Koczkur, S. Mourdikoudis, L. Polavarapu, and S. E. Skrabalak, Dalton Trans. 44 (2015) 17883.
[43] I. Karimzadeh, M. Aghazadeh, M. R. Ganjali, P. Norouzi, and S. S. Arani, Mater. Lett. 179 (2017) 5.